Colloids and Surfaces A: Physicochem. Eng. Aspects 489 (2016) 173–181

Contents lists available at ScienceDirect

Colloids and Surfaces A: Physicochemical and Engineering Aspects

journal homepage: www.elsevier.com/locate/colsurfa

Photodegradation behavior of poly(butylene succinate-co-butylene adipate)/ZnO nanocomposites

Yang Zhang, Jun Xu, Baohua Guo*

Key Laboratory of Advanced Materials of Ministry of Education, Department of Chemical Engineering, Tsinghua University, Beijing 100084, China

HIGHLIGHTS

- ZnO nanoparticles are well distributed and dispersed in PBSA matrix.
- FT-IR, PGC-MS, DSC and SEM are used to characterize the photodegradation behavior.
- ZnO can stabilize the PBSA matrix during photodegradation.
- The possible structure of degradation products are analyzed using PGC-MS.

GRAPHICAL ABSTRACT

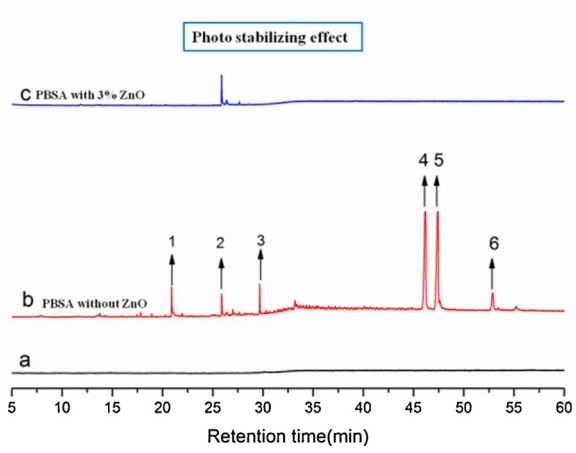

ARTICLE INFO

Article history:
Received 10 July 2015
Received in revised form 14 October 2015
Accepted 23 October 2015
Available online 28 October 2015

Keywords:
Biodegradable polymer
Poly(butylene succinate-co-butylene adipate)
ZnO
Nanocomposites
Photodegradation behavior

ABSTRACT

The photodegradation of PBSA and PBSA/ZnO nanocomposites with different ZnO loadings were studied in this paper. The PBSA/ZnO nanocomposites were prepared by melt-compounding process and the ZnO dispersion state within the PBSA matrix was analyzed by TEM. The reduction of molecular weight of PBSA nanocomposites is lower than that of the neat PBSA, which indicates more chain scission occured in neat PBSA. The chemical structure changes characterized by FTIR and PGC-MS showed that ZnO nanoparticles can stabilize the PBSA matrix. Carbonyl index and hydroxyl index of PBSA grew more significantly than PBSA nanocomposites. More degradation products accumulated in PBSA samples than in the PBSA nanocomposite samples. Thermal properties analyzed by DSC revealed a decrease of crystallization temperature in all samples, which is due to the formation of short chains after irradiation. In addition, the small fragments could recrystallize and increase the crystallinity. SEM images of sample surfaces revealed that PBSA sample had severer damages on surface than PBSA/ZnO nanocomposites. These results demonstrate that ZnO nanoparticles can hinder the photodegradation of PBSA.

1. Introduction

In recent years, biodegradable polymers gained wide attention because of their potential to minimize the environmental

* Corresponding author.
E-mail address: bhguo@mail.tsinghua.edu.cn (B. Guo).

http://dx.doi.org/10.1016/j.colsurfa.2015.10.038
0927-7757/

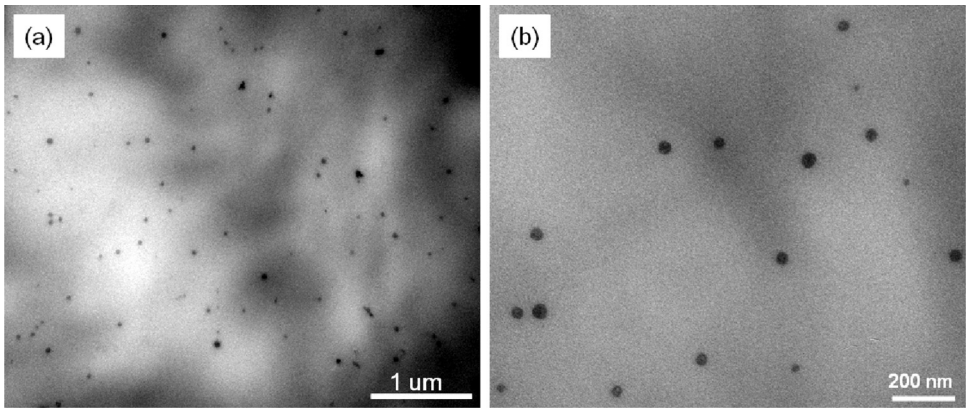

Fig. 1. (a, b) TEM images at different magnifications of PBSA-1 nanocomposite.

problems caused by the disposal of non-biodegradable polymers [1,2]. A variety of biodegradable polymers have been studied such as poly(butylene succinate) (PBS) [3], poly(lactic acid) (PLA) [4], poly(ϵ-caprolactone) (PCL) [5], polyhydroxyalkanoates (PHA) [6] and poly(butylene adipate-co-butylene terephthalate) (PBAT) [7]. Among the biodegradable polymers, poly(butylene succinate-co-butylene adipate) (PBSA), chemically synthesized by the polycondensation of 1,4-butanediol, succinic acid and adipic acid, plays an important role in the biodegradable polymer field for its biomass-based resource, appropriate degradation rate, thermal stability, mechanical property and good processability [2,5,7]. As a result, it has found applications in biodegradable fibers, packaging materials, injection molded products and mulch films. For some outdoor applications of PBSA-based materials (e.g., mulch films), photodegradation stability is a crucial property in its practical use. So, studies associated with photodegradation of PBSA and its composite are vital in order to predict their life-time and behavior in outdoor applications.

The utilization of nanoscale materials is an emerging area for many applications. Various nanosized materials have been used to prepare biodegradable polymer nanocomposite to improve physical properties of polymer composites [8–12]. Nanoparitlces such as titanium dioxide (TiO_2), silicon oxide (SiO_2), aluminium oxide (Al_2O_3), and zinc oxide (ZnO) can act as inorganic UV-screen agents and have influences on the photodegradation behavior of polymer matrix. Yang et al. [13] compared the impact of different nanoparticles (SiO_2, Al_2O_3, ZnO) on linear low density polyethylenes (LLDPE) and found that all the three nanopartilces can improve the photo stability of the composites. Miyauchi et al. [14] revealed that photo decomposition of PBS depended on the size and dispersibility of TiO_2 and would enhance the degradation of PBS/TiO_2 composite under sunlight. The similar conclusion was drawn in PLA/TiO_2 composite by Nakayama and Hayashi [15]. It has been reported that ZnO is not only a UV-screen agent but also an antibacterial multifunctional material. Several works [16–19] have reported the photodegradation behavior of polyolefin and polyester when ZnO was incorporated into polymer matrix. However, only a few papers noted ZnO filled biodegradable polymers. Liu et al. [20] showed the effect surface modification of ZnO on mechanical and crystallization performances of PBS/ZnO composite. Therias et al. [21] studied the photochemical behavior of PLA/ZnO nanocomposite films.

In this work, PBSA/ZnO nanocomposites were prepared by melt-compounding process and the effect of ZnO nanoparticles on the photodegradation behavior of PBSA/ZnO nanocomposites was investigated and compared to the behavior of pristine PBSA. Chemical, thermal and morphological property changes were evaluated on the composites and discussed as a function of irradiation time.

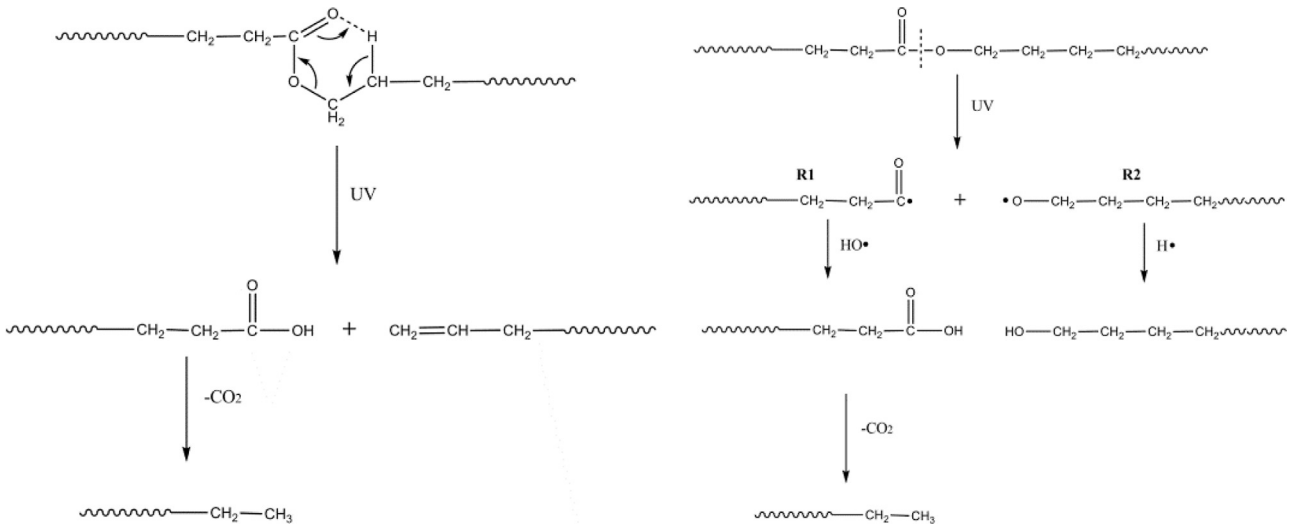

Scheme 1. Route of PBSA photodegradation.

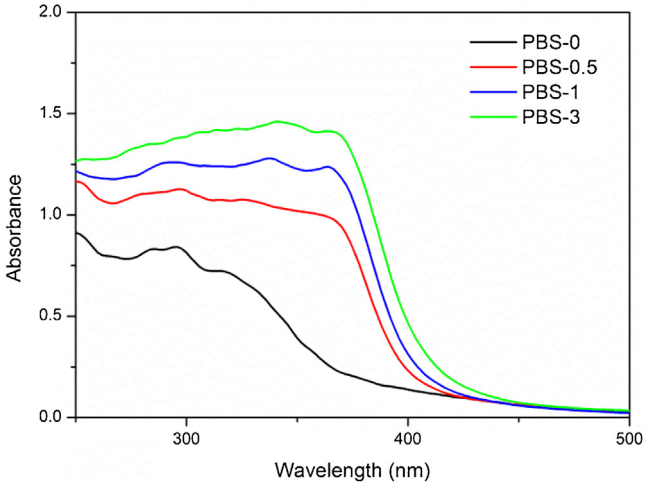

Fig. 2. UV–visible spectra of neat PBSA and PBSA/ZnO nanocomposites before irradiation.

2. Experimental

2.1. Materials

Poly(butylene succinate-co-butylene adipate) (melting temperature = 111.9 °C, melt flow index = 23.2 g/10 min) was supplied by Xinjiang Blue Ridge Tunhe Polyester Co., Ltd., China. The composition of the original PBSA before aging test was calculated by ^{1}H NMR: the molar ratio of adipate unite to succinate unite was 2.48%. ZnO nanoparticles with diameter of 30 ± 10 nm were supplied by Aladin chemistry Co., Ltd., China. All materials were used as received.

2.2. Preparation of PBSA/ZnO nanocomposites

The PBSA/ZnO nanocomposites were produced by melt-compounding PBSA with up to 3 wt% ZnO nanoparticles in a HAAKE PolyLab mixer (Thermo Electron Co.). Briefly, the fabrication of PBSA/ZnO nanocomposite with 0.5 wt% ZnO content was described as follows: 49.75 g previously dried pellets of PBSA were added into HAAKE mixer at 140 °C for 3 min for premelting. Then, 0.25 g ZnO was added into the melt and mixed for another 10 min. Other nanocomposites containing 1 and 3 wt% were produced in the same procedure and homogeneous PBSA was also processed at the same condition as a reference sample. The PBSA/ZnO nanocomposites and unfilled PBSA were hot-pressed to films of ~100 μm in thickness and plates of 2 mm in thickness. For brevity, PBSA nanocomposites with 0, 0.5, 1 and 3 wt% ZnO loadings are denoted as PBSA-0, PBSA-0.5, PBSA-1 and PBSA-3, respectively.

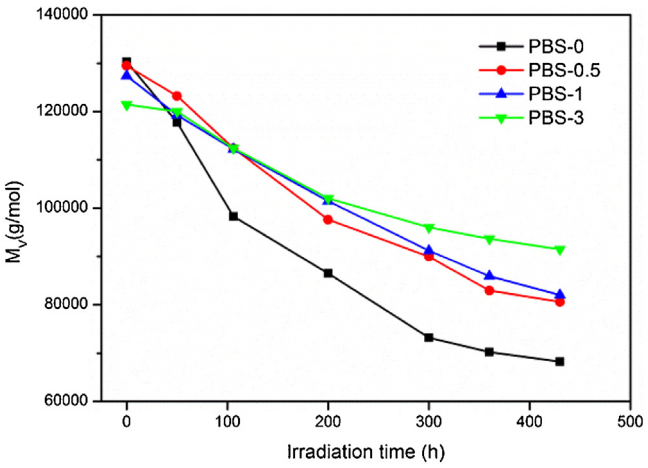

Fig. 3. Changes of molecular weight of neat PBSA and PBSA/ZnO nanocomposites as a function of irradiation time.

2.3. Artificial aging test

The film samples and plate samples were irradiated under accelerated artificial conditions. The aging device was a Q-SUN xenon test chamber (model Xe-3-HS) from Q-Lab Co., (USA), which was equipped with three xenon arc lamps. Wavelength below 300 nm were filtered by the glass envelops of the source. The spectrum of lamp is shown in supplementary data (Fig. S1). The temperature of chamber air was fixed at 38 °C. The relative humidity (RH) of the chamber is 30%.

2.4. Characterizations

The transmission electron microscopy analysis (TEM) was conducted using a Hitachi H-7650B instrument (Japan) using an accelerator voltage of 80 kV. For TEM investigations, the nanocomposite samples were prepared with a Leica EMUC 6 microtoming (Germany) by cutting at −80 °C. Reported microphotographs represent typical morphologies as observed, at least, three different locations of the sample.

The surface morphologies of samples were examined by a JSM-7401 field emission scanning electron microscopy (FESEM) at an accelerating voltage of 3 kV. All samples were covered with platinum prior to the examination.

The Fourier transform infrared (FTIR) spectra were obtained using a Bruker V70 Hyper1000 (Germany). For films, transmission spectra were obtained by signal averaging 32 scans at the resolution of 4 cm^{-1} in the wavenumber range of 400–4000 cm^{-1}. The attenuated total reflection (ATR) technique was also used to determine the surface changes of samples in the wavenumber range of 600–4000 cm^{-1}, with diamond as the ATR crystal. Film samples were analyzed using transmission mode and plate samples were analyzed using ATR mode. Peak at 2856 cm^{-1} was used as reference, which is associated with the C—H stretching [22]. The area ratio of carbonyl absorbance to reference is defined as carbonyl index ($A_{C=O}/A_{-CH}$) and the area ratio of hydroxyl absorbance to reference is defined as hydroxyl index (A_{-OH}/A_{-CH}). UV–visible spectra were recorded on a Hitachi U-3010 spectrophotometer (Japan) equipped with an integrating sphere for diffuse reflection in the wavelength range of 200–500 nm.

Differential scanning calorimetry (DSC) analysis was carried out to study the thermal behavior of samples using a Shimadzu DSC-60 (Japan) equipment. The samples were heated from 30 °C to 160 °C at a heating rate of 10 °C/min and held for 3 min to eliminate the thermal history. Then, samples were cooled to 30 °C at a rate of 10 °C/min. The crystallinity of PBSA and its nanocomposites was calculated by the function $X_c = \left[\left(\Delta H_m/\Delta H_m^0\right)/\phi\right] \times 100\%$, where ΔH_m is the melting enthalpy of the sample and ΔH_m^0 is the melting enthalpy of 100% crystalline PBSA (ΔH_m^0 = 110.5 J/g [23]); φ is the weight percentage of PBSA in matrix.

Molar mass values of samples were calculated from viscosity measurements. The inherent viscosities were measured with a Ubbelhode viscometer at 25 °C in 1:1 (w/w) phenol/tetrachchloroethane solution. The Mark–Houwink equation was used to calculate the M_v values ($[\eta] = KM_v^\alpha$, $K = 1.71 \times 10^{-4}$, $\alpha = 0.79$) [24].

The volatile photodegradation products of neat PBSA and its composite were analyzed by a pyrolysis gas chromatograph-mass spectrometer (PGC-MS) (Shimadzu GCMS-QP5050A equipped with

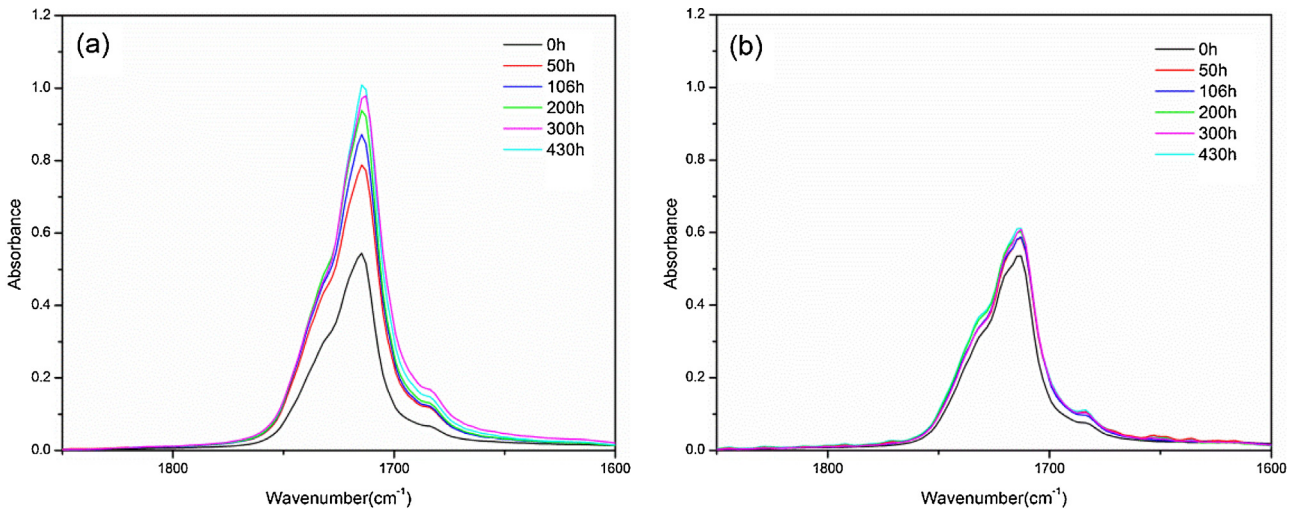

Fig. 4. FTIR ATR spectra of (a) PBSA-0 and (b) PBSA-3 from 0 to 430 h of irradiation in the region of 1600–1850 cm^{-1}.

PYR 4A pyrolyzer). The flash evaporation technique was used to separate chain scission-induced small molecules from the polymers. About 1 mg sample was flash-heated at 300 °C for 30 s. The mixture of small molecules was carried through the fused silica capillary column (DB-5 25 μm × 0.25 mm i.d.) by the carrier gas He and separated at the same time. Each component was detected by the MS detector.

3. Results and discussion

3.1. Characterization of PBSA/ZnO nanocomposites

3.1.1. Transmission electron microscopy (TEM)

Most properties of nanocomposites are related to the dispersion degree of nanoparticles in polymer matrix. Fig. 1 shows TEM images of PBSA/ZnO nanocomposite at different magnifications. The TEM images reveal that the ZnO nanoparticles are well-distributed and dispersed through the PBSA matrix without showing noticeable aggregates. The good dispersity of ZnO in PBSA can be attributed to the high sheer forces applied in the melt-compounding process. The TEM image of PBSA-3 are also provided (Fig. S2) in Supplementary data file.

3.1.2. UV–visible spectroscopy

The UV–visible spectra of neat PBSA and PBSA/ZnO nanocomposites with different ZnO content before irradiation are presented in Fig. 2. In the UV–visible spectrum of neat PBSA, a relatively weak absorption occurs in the spectral region of 250–350 nm, which is attributed to the absorption of carbonyl group. For all of the samples with ZnO nanoparticles, an absorption resulting from the presence of ZnO is observed in the domain up to 400 nm.

3.2. Photodegradation of nanocomposites

3.2.1. Molecular weight characterization

In order to evaluate the effect of ZnO nanoparticles on the PBSA photodegradation, analysis of the evolution of the molecular weight of neat PBSA and PBSA/ZnO nanocomposites during photodegradation was carried out and the results are presented in Fig. 3. Before irradiation, all samples show slight decrease in molecular weight, which indicates the degradation of PBSA caused by the different level of shear stress and thermal degradation during melt-mixing and processing [25,26]. In any case, the reduction in molecular weight due to the melt process is less than 10%.

From Fig. 3, it can be observed that the photodegradation causes obvious reduction in molecular weight in all samples. As previously reported [27], this decrease indicates that photodegradation of

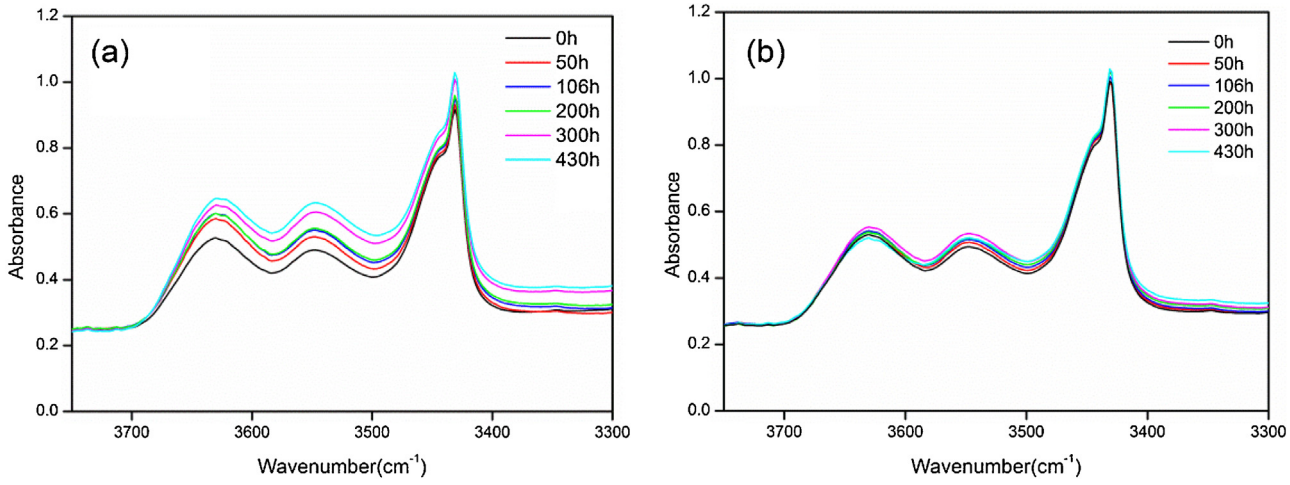

Fig. 5. FTIR transmission spectra of (a) PBSA-0 and (b) PBSA-3 from 0 to 430 h of irradiation in the region of 3300–3800 cm^{-1}.

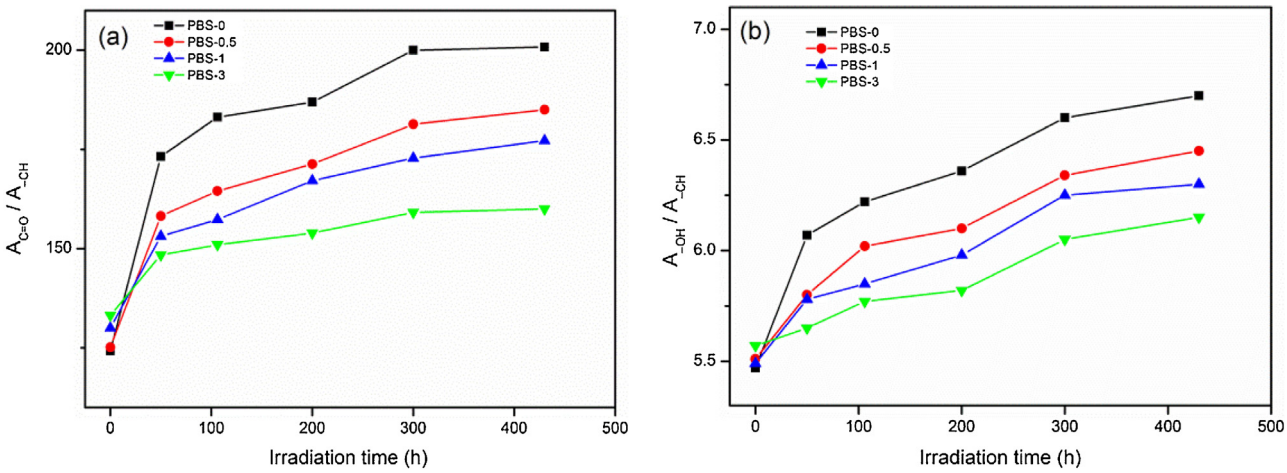

Fig. 6. Changes of carbonyl index (a) and hydroxyl index (b) of neat PBSA and PBSA/ZnO nanocomposites as a function of irradiation time.

PBSA provokes chain scissions, which leads to the formation of low molecular weight products. However, the reduction rates of samples are different. The reduction rate of molecular weight decreases with increasing the ZnO content. The reduction of molecular weight for neat PBSA is higher than 50% after 430 h irradiation. As contrast, after 430 h irradiation, the molecular weight of PBSA matrix was reduced by approximately 35, 38 and 25% in the presence of 0.5, 1 and 3% ZnO nanopariticles, respectively.

3.2.2. FTIR spectroscopic characterization

The chemical modifications resulting from photodegradation were monitored using IR spectroscopy. Figs. 4 and 5 show IR spectra of PBSA-0 and PBSA-3 in two different regions, i.e., 1600–1850 cm^{-1} and 3300–3800 cm^{-1}, before and after different exposure time. The carbonyl stretching band appears at 1715 cm^{-1} and the broad band between 3380 and 3700 cm^{-1} is ascribed to hydroxyl stretching [22].

Based on the structure of PBSA, hydroxyl (OH) and carbonyl (C=O) groups can be used as tools to study degradation [28]. For PBSA-0, the carbonyl peaks increased and broadened with increasing exposure time. This suggests the formation of other carbonyl species which may include free C=O and C=O from carboxyl acid groups [29]. In the region from 3300 to 3800 cm^{-1}, an intense increase in OH groups for PBSA-0 is observed (Fig. 5a). As a result of hydroxyl end groups oxidation and main chain scission from photolysis at ester linkages [28,29], terminal hydroxyl and carboxyl acid groups are generated, so as irradiation progresses, an increase in OH groups is observed in the IR spectra. The IR spectra of PBSA-3 show slight increases in the carbonyl domain (Fig. 4a) and hydroxyl domain (Fig. 5a). These results indicate that the similar PBSA photodegradation products formed for pure PBSA and PBSA nanocomposites and the ZnO nanoparticles has no influence on the mechanism of PBSA photodegradation process. The second question concerns the effect of the nanoparticles on the rate of photodegradation of PBSA. Fig. 6 shows the changes of carbonyl index and hydroxyl index of neat PBSA and PBSA/ZnO nanocomposites as a function of irradiation time. Several conclusions can be made according to these results. First, no induction period was observed for all samples during the photodegradation process and photodegradation products accumulated from the beginning of irradiation. Once the irradiation process starts, photodegradation process starts immediately regardless of what the ZnO content is. Second, the carbonyl index and hydroxyl index of neat PBSA are higher than that of PBSA nanocomposites at any identical irradiation time. This means that the rate of degradation of PBSA decreases with the amount of ZnO, which suggests that ZnO has a stabilizing effect under conditions of photodegradation.

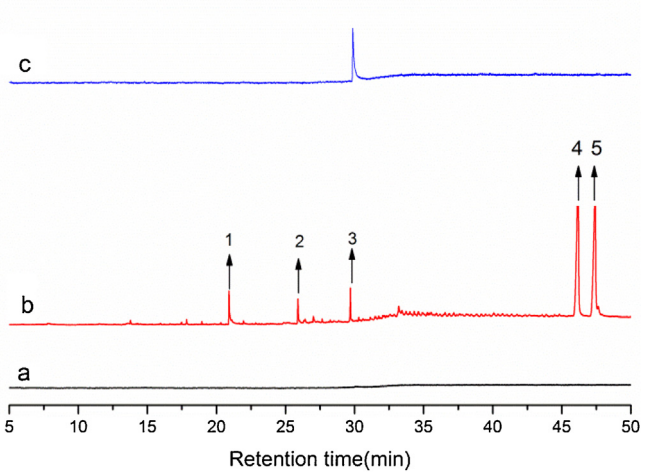

Fig. 7. PGC-MS pyrograms of PBSA and PBSA nanocomposite before and after exposure. (a) PBSA-0 before exposure; (b) PBSA-0 after exposure; (c) PBSA-3 after exposure.

3.2.3. PGC-MS characterization

The pyrolysis gas chromatograph-mass spectrometer (PGC-MS) was carried out to investigate the volatile degradation products after photodegradation (Fig. 7). No peaks are present in PBSA-0 and PBSA-3 before exposure. After exposure, some volatile small molecule fragments formed in PBSA nanocomposite as shown in Fig. 7b. The possible attributions of characteristic peaks are shown in Table 1. The main volatile degradation products are esters compounds, alcohols and unsaturated materials, which containing succinate unite, adipate unite or 1,4-butandiol unite. During photodegradation, PBSA molecular chains undergo both formation of carboxyl end groups and chain scission which are presented in Scheme 1. PBSA molecular chains can degrade through a six-membered transition state around ester linkages, leading to the formation of a carboxylic acid and a double bond [30–32]. Furthermore, the terminal carboxyl group may undergo a decarboxylation process during the irradiation. At the same time, PBSA chains can also decompose by the homolysis of the ester bond. This reaction produces radicals R_1 and R_2. The reaction of R_1 with hydroxyl radicals OH produces carboxylic acid and the reaction of R_2 with hydrogen radicals leads to the formation of alcohols.

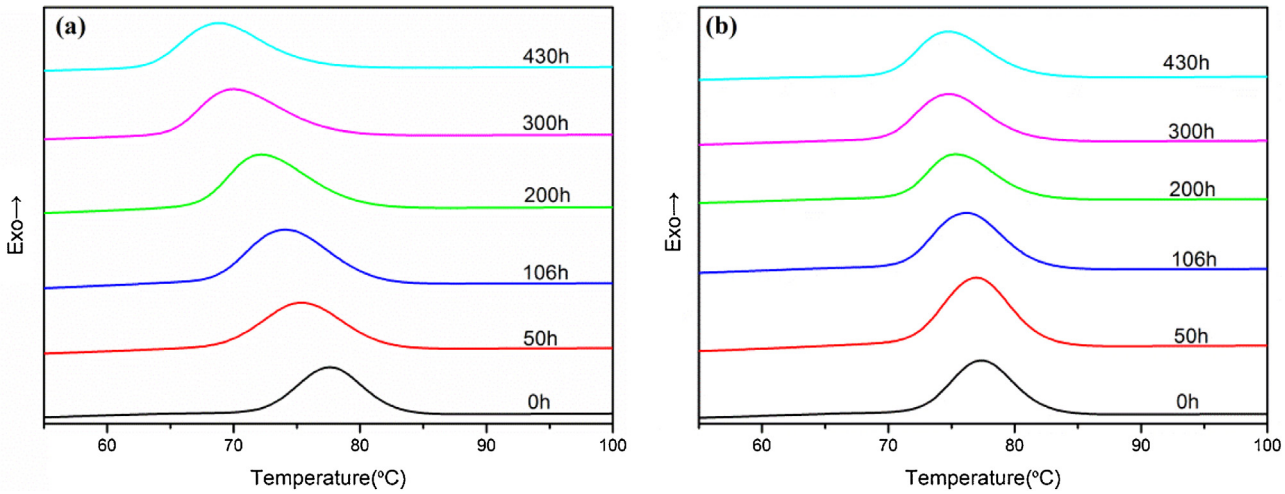

Fig. 8. DSC curves of (a) PBSA-0 and (b) PBSA-3 during cooling from the melt at a rate of 10 °C/min at different irradiation time.

Compared to PBSA-0, a quite low fragment amount appeared in the PGC-MS pyrogram of PBSA-3. This result suggests that pure PBSA underwent a more significant photodegradation than PBSA nanocomposites. Although chain scission and oxidation occurred in PBSA-3 sample according to results listed above, only a small amount of fragments generated in the matrix and small molecular fragments tend to diffuse into the atmosphere as time passed. That is to say, even though there are some volatile fragments generated, these products might not stay in the PBSA-3 samples. Therefore, volatile fragments accumulated in PBSA-3 matrix are almost undetectable because PGC-MS analysis mainly focused on the volatile products present in polymer matrix, which is shown in Fig. 7c.

3.2.4. Thermal properties

The thermal properties of neat PBSA and PBSA/ZnO nanocomposites detected by DSC are summarized in Table 2. Fig. 8 presents the crystallization curves of PBSA-0 and PBSA-3 at different irradiation time. For neat PBSA (Fig. 8a), the crystallization temperature (T_c) has a significant reduction from 77.5 °C to 68.8 °C after 430 h of irradiation. Yet T_c of PBSA-3 decreased slightly from 77.4 °C to 74.7 °C after the same irradiation time. Fig. 9 shows changes of crystallization temperature of neat PBSA and PBSA/ZnO nanocomposites as a function of irradiation time. It reveals that the reduction of crystallization temperature decreases with increasing the ZnO loadings. As the samples exposed to irradiation, long chains of polymer break into relatively short chains which have better chain mobility. Therefore, short chains have the ability to orient into an ordered structure intramolecularly or intermolecularly at a lower temperature compared to long molecular chains. In addition, more chain entanglements which can act as nuclei may exist in PBSA/ZnO nanocomposites possessing longer molecular chains. So PBSA/ZnO nanocomposites have higher crystallization temperature during the cooling process.

Changes of melting temperature (T_m) and crystallinity are shown in Table 2. T_m of all samples show little changes while all samples have an increase of crystallinity after 430 h of irradiation. The crystallinity of all samples are the same before irradiation. After

Table 1
The possible chemical structure of volatile products in Fig. 7.

Peak	Attribution
1	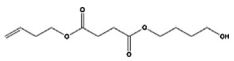
2	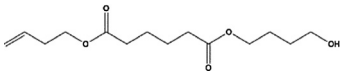
3	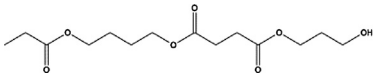
4, 5	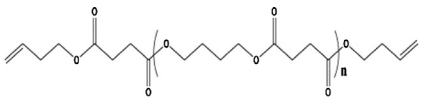

Table 2
Thermal parameters of PBSA and PBSA nanocomposites at different irradiation time.

Sample	Time (h)	T_m (°C)	T_c (°C)	Crystallinity (%)
PBSA-0	0	111.1	77.5	44.5
	200	111.7	72.2	55.9
	430	111.7	68.8	57.4
PBSA-0.5	0	111.5	78.7	44.2
	200	111.9	74.3	51.6
	430	111.7	73.5	52.7
PBSA-1	0	111.7	78.1	45.0
	200	111.9	75.3	47.4
	430	111.7	73.7	52.4
PBSA-3	0	111.7	77.2	45.5
	200	111.5	75.4	46.6
	430	111.9	74.7	50.9

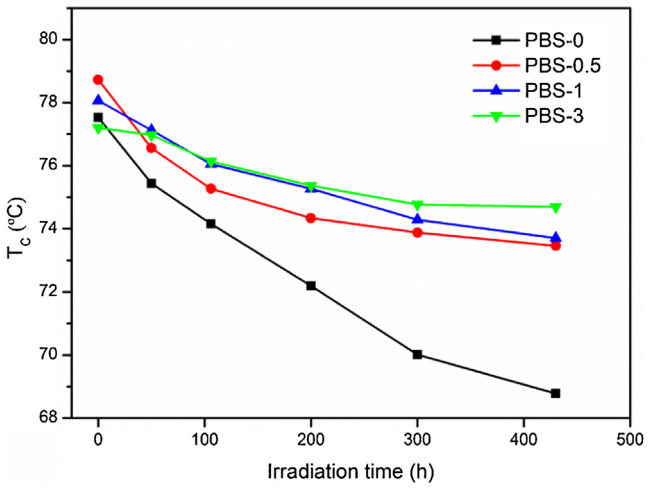

Fig. 9. Changes of crystallization temperature of neat PBSA and PBSA/ZnO nanocomposites as a function of irradiation time.

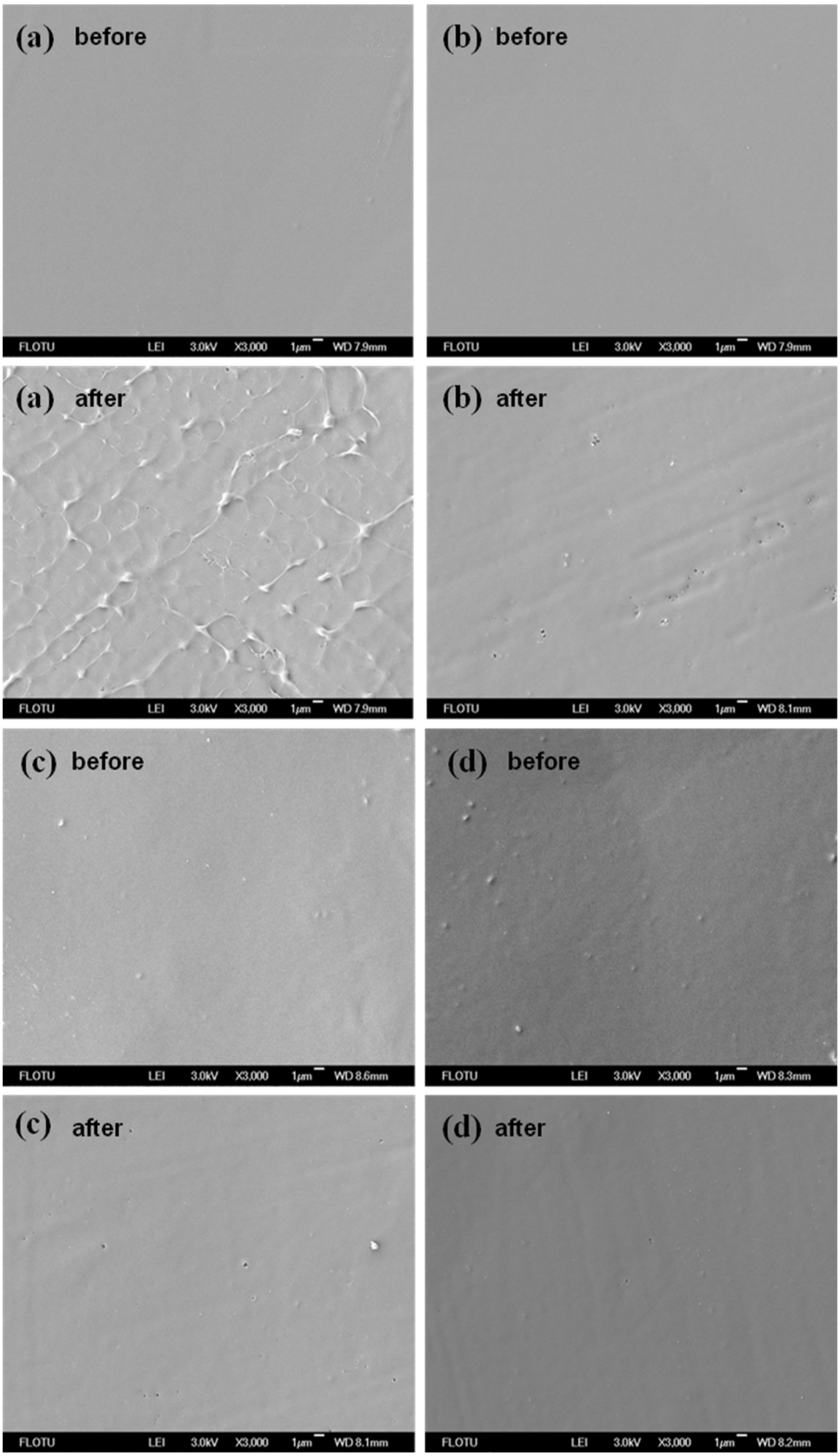

Fig. 10. The surface changes of (a) PBSA-0, (b) PBSA-0.5, (c) PBSA-1 and (d) PBSA-3 by SEM.

430 h of aging test, the increase of crystallinity of PBSA-0, PBSA-0.5, PBSA-1 and PBSA-3 is 13.0%, 8.5%, 7.4% and 5.0%, respectively. This increase is mainly due to the degradation of PBSA chains in the amorphous regions because the amorphous region is more accessible to degrade. During irradiation, polymer molecular weight reduced owing to chain scission, which is in favor of polymer crys-

tallization. Chain scission could release the previously entangled polymer chains in the amorphous region. Then the shorter PBSA segments, possessing higher mobility, can reorganize into crystalline phase, which leads to an increase of crystallinity. Pegoretti and Penati [33] reported this phenomenon as chemicrystallization, which is widely observed in semicrystalline aliphatic polyesters. During irradiation, a greater extent of chain scission led to a greater increase in crystallinity for PBSA-0.

3.2.5. Morphological properties

SEM analysis was conducted on the surface of sample films in order to investigate morphological changes caused by photoaging and then understand the influence of surface change on the photodegradation of PBSA matrix. Fig. 10 shows the surfaces of neat PBSA and PBSA/ZnO nanocomposites films before and after more than 400 h of irradiation. Before exposure, neat PBSA film exhibits a smooth and clear surface with no significant defects and PBSA nanocomposite films exhibit clear surface with some particles embedded in the polymer matrix. After 430 h of irradiation, the surface of neat PBSA film is very rough and characterized with many tiny pores. In contrast, the surfaces of PBSA/ZnO nanocomposites films remain smooth with several tiny pores. The morphology characterization indicates that surface of PBSA composite is less damaged than surface of neat PBSA because of the presence of ZnO and the surface changes are consistent with results listed above. It is understandable that the photodegradation of polymer films begins from the surface and then develops along the depth gradually [34]. As a result, the bulk degradation of polymer is directly related to the surface photodegradation pattern. The degradation will be restricted to a thin layer at the surface if the surface damage is not severe. However, a serious oxidation surface provides a path for the oxygen to get into the interior of the material, thus causing further degradation of the bulk.

4. Conclusions

In this work, the photodegradation behavior of PBSA modified with different ZnO content was studied and the effect of ZnO nanaoparticles on the stability of PBSA matrix was investigated. The results of chemical structure revealed that ZnO nanoparticles can stabilize PBSA matrix. The higher ZnO loadings, the slower the PBSA degraded. However, the photodegradation mechanism of PBSA did not change significantly. Thermal properties analysis showed a decrease of crystallization temperature and an increase of crystallinity of all samples due to the formation of short chains and decrease of entangled chain segments. Furthermore, SEM micrographs indicated an extended decomposition for the surface of neat PBSA where as PBSA nanocomposites samples showed limited surface degradation.

Acknowledgements

The authors thank the National Natural Science Foundation of China (Grant No. 21274077, 51473085) and the National High-Tech R&D Program of China (863 Program) (Grant No. 2011AA02A203) for the financial support of this work.

Appendix A. Supplementary data

Supplementary data associated with this article can be found, in the online version, at http://dx.doi.org/10.1016/j.colsurfa.2015.10.038.

References

[1] M.M. Reddy, S. Vivekanandhan, M. Misra, S.K. Bhatia, A.K. Mohanty, Biobased plastics and bionanocomposites: current status and future opportunities, Prog. Polym. Sci. 38 (2013) 1653–1689.
[2] J. Xu, B.-H. Guo, Poly(butylene succinate) and its copolymers: research, development and industrialization, Biotechnol. J. 5 (2010) 1149–1163.
[3] Z. Gan, H. Abe, H. Kurokawa, Y. Doi, Solid-state microstructures, thermal properties, and crystallization of biodegradable poly(butylene succinate) (PBS) and its copolyesters, Biomacromolecules 2 (2001) 605–613.
[4] K. Fukushima, Y. Kimura, Stereocomplexed polylactides (Neo-PLA) as high-performance bio-based polymers: their formation, properties, and application, Polym. Int. 55 (2006) 626–642.
[5] E. Chiellini, R. Solaro, Biodegradable polymeric materials, Adv. Mater. 8 (1996) 305–313.
[6] G.-Q. Chen, A microbial polyhydroxyalkanoates (PHA) based bio- and materials industry, Chem. Soc. Rev. 38 (2009) 2434–2446.
[7] A.A. Shah, F. Hasan, A. Hameed, S. Ahmed, Biological degradation of plastics: a comprehensive review, Biotechnol. Adv. 26 (2008) 246–265.
[8] S. Sinha Ray, M. Bousmina, Biodegradable polymers and their layered silicate nanocomposites: in greening the 21st century materials world, Prog. Mater. Sci. 50 (2005) 962–1079.
[9] S.-R. Lee, H.-M. Park, H. Lim, T. Kang, X. Li, W.-J. Cho, C.-S. Ha, Microstructure, tensile properties, and biodegradability of aliphatic polyester/clay nanocomposites, Polymer 43 (2002) 2495–2500.
[10] J. Ramontja, S.S. Ray, S.K. Pillai, A.S. Luyt, High-performance carbon nanotube-reinforced bioplastic, Macromol. Mater. Eng. 294 (2009) 839–846.
[11] S.Y. Hwang, E.S. Yoo, S.S. Im, The synthesis of copolymers, blends and composites based on poly(butylene succinate), Polym. J. 44 (2012) 1179–1190.
[12] X.W. Wang, C.A. Zhang, P.L. Wang, J. Zhao, W. Zhang, J.H. Ji, K. Hua, J. Zhou, X.B. Yang, X.P. Li, Enhanced performance of biodegradable poly(butylene succinate)/graphene oxide nanocomposites via in situ polymerization, Langmuir 28 (2012) 7091–7095.
[13] R. Yang, Y. Li, J. Yu, Photo-stabilization of linear low density polyethylene by inorganic nano-particles, Polym. Degrad. Stab. 88 (2005) 168–174.
[14] M. Miyauchi, Y. Li, H. Shimizu, Enhanced degradation in nanocomposites of TiO_2 and biodegradable polymer, Environ. Sci. Technol. 42 (2008) 4551–4554.
[15] N. Nakayama, T. Hayashi, Preparation and characterization of poly(l-lactic acid)/TiO_2 nanoparticle nanocomposite films with high transparency and efficient photodegradability, Polym. Degrad. Stab. 92 (2007) 1255–1264.
[16] H. Zhao, R.K.Y. Li, A study on the photo-degradation of zinc oxide (ZnO) filled polypropylene nanocomposites, Polymer 47 (2006) 3207–3217.
[17] O.H. Lin, H.M. Akil, S. Mahmud, Effect of particle morphology on the properties of polypropylene/nanometric zinc oxide composites, Adv. Compos. Lett. 18 (2009) 77–83.
[18] S. Chandramouleeswaran, S.T. Mhaske, A.A. Kathe, P.V. Varadarajan, V. Prasad, N. Vigneshwaran, Functional behaviour of polypropylene/ZnO-soluble starch nanocomposites, Nanotechnology 18 (2007) 385702.
[19] J. He, W. Shao, L. Zhang, C. Deng, C. Li, Crystallization behavior and UV-protection property of PET-ZnO nanocomposites prepared by in situ polymerization, J. Appl. Polym. Sci. 114 (2009) 1303–1311.
[20] W.-G. Liu, X.-C. Zhang, H.-Y. Li, Z. Liu, Effect of surface modification with 3-aminopropyltriethyloxy silane on mechanical and crystallization performances of ZnO/poly(butylenesuccinate) composites, Compos. Part B: Eng. 43 (2012) 2209–2216.
[21] S. Therias, J.-F. Larché, P.-O. Bussière, J.-L. Gardette, M. Murariu, P. Dubois, Photochemical behavior of polylactide/ZnO nanocomposite films, Biomacromolecules 13 (2012) 3283–3291.
[22] Z. Qi, H. Ye, J. Xu, J. Peng, J. Chen, B. Guo, Synthesis and characterizations of attapulgite reinforced branched poly(butylene succinate) nanocomposites, Colloids Surf., A 436 (2013) 26–33.
[23] Y.-R. Tang, D.-W. Lin, Y. Gao, J. Xu, B.-H. Guo, Prominent nucleating effect of finely dispersed hydroxyl-functional hexagonal boron nitride on biodegradable poly(butylene succinate), Ind. Eng. Chem. Res. 53 (2014) 4689–4696.
[24] X. Liu, G. Huang, S. Wang, Synthesis of high molecular weight poly(butylene succinate) and relationship of molecular weight with intrinsic viscosity, Chin. Plast. Ind. 36 (2008) 14–16.
[25] G. Gorrasi, A. Sorrentino, Photo-oxidative stabilization of carbon nanotubes on polylactic acid, Polym. Degrad. Stab. 98 (2013) 963–971.
[26] Y.J. Phua, W.S. Chow, Z.A. Mohd Ishak, The hydrolytic effect of moisture and hygrothermal aging on poly(butylene succinate)/organo-montmorillonite nanocomposites, Polym. Degrad. Stab. 96 (2011) 1194–1203.
[27] M. Gardette, S. Thérias, J.-L. Gardette, M. Murariu, P. Dubois, Photooxidation of polylactide/calcium sulphate composites, Polym. Degrad. Stab. 96 (2011) 616–623.
[28] T. Kijchavengkul, R. Auras, M. Rubino, S. Selke, M. Ngouajio, R.T. Fernandez, Biodegradation and hydrolysis rate of aliphatic aromatic polyester, Polym. Degrad. Stab. 95 (2010) 2641–2647.
[29] S. Carroccio, P. Rizzarelli, C. Puglisi, G. Montaudo, MALDI investigation of photooxidation in aliphatic polyesters: poly(butylene succinate), Macromolecules 37 (2004) 6576–6586.

[30] T. Kijchavengkul, R. Auras, M. Rubino, E. Alvarado, J.R. Camacho Montero, J.M. Rosales, Atmospheric and soil degradation of aliphatic–aromatic polyester films, Polym. Degrad. Stab. 95 (2010) 99–107.
[31] S. Bocchini, K. Fukushima, A.D. Blasio, A. Fina, A. Frache, F. Geobaldo, Polylactic acid and polylactic acid-based nanocomposite photooxidation, Biomacromolecules 11 (2010) 2919–2926.
[32] H. Tsuji, Y. Echizen, Y. Nishimura, Photodegradation of biodegradable polyesters: a comprehensive study on poly(l-lactide) and poly(ϵ-caprolactone), Polym. Degrad. Stab. 91 (2006) 1128–1137.
[33] A. Pegoretti, A. Penati, Recycled poly(ethylene terephthalate) and its short glass fibres composites: effects of hygrothermal aging on the thermo-mechanical behaviour, Polymer 45 (2004) 7995–8004.
[34] R. Yang, J. Yu, Y. Liu, K. Wang, Effects of inorganic fillers on the natural photo-oxidation of high-density polyethylene, Polym. Degrad. Stab. 88 (2005) 333–340.